Algorithms for Automated Characterization of Three-Axis Stabilized GEOs using Non-Resolved Optical Observations

Jeremy Murray-Krezan
AFRL Space Vehicles Directorate
Willa C. Inbody
AFRL Space Vehicles Directorate
Phan Dao
AFRL Space Vehicles Directorate
Anthony Dentamaro
Boston College
Daniel Fulcoly
AFRL Space Vehicles Directorate
Stephen A. Gregory
Boeing Corp.

Non-resolved optical observations of satellites have been known to supply researchers with valuable information about satellite status. Until recently most non-resolved analysis techniques have required an expert human in the loop in order to attribute observed information to satellite features. We are designing algorithms that automate the process of rapidly characterizing satellites from non-resolved optical data of 3-axis stabilized geostationary satellites. We will present background information on corrections for lighting conditions that vary as a function of the Earth's season, and permit automated satellite characterization algorithms. Much of this information is empirical, based on a GEO-Sat Color Photometry Catalog (GCPC), for which collection began in 2004 and continues into the present.

1. INTRODUCTION

Observation of the brightness of 3-axis stabilized GEO stationary satellites as a function of time supplies valuable information on the satellite type, size, characteristics, and state [1-4]. Since traditional telescopes are too limited in spatial acuity to resolve satellites at GEO-belt distances, inferences must be made by observing the brightness of the space object. In this paper, we describe how that brightness may vary as a function of time, and more specifically the Earth's seasons.

Analysis of multi-filter photometric observations of approximately 115 GEO satellites gathered over the last 8 years has led to a qualitative understanding of the effects that seasonal illumination changes cause when looking at the reflected sunlight from stable satellites [4]. These changes are most easily understood if one considers the common fixed reference frame that includes the sensor and the satellite body. In this frame, the sun completes an azimuthally aligned circle around the satellite in a 24 hour period, and the solar panels articulate in order generally to follow the sun. On a seasonal time scale, one must also add the apparent north/south (n/s) component of illumination change as the sun appears to be on the Celestial Equator at the two equinoxes and has maximum value, 23.44^{o}, excursions at the solstices (see Fig. 1).

In this paper, we demonstrate an empirical model for describing the seasonal effects in a light curve, or time-dependent satellite brightness, and interpret changes in measured light curves using this empirical model. We also show results that hint at the necessity to include seasonal, orbital, and lighting condition effects into light curve analysis and detailed models, such as those of TASAT, OSC, or other similar satellite modeling efforts.

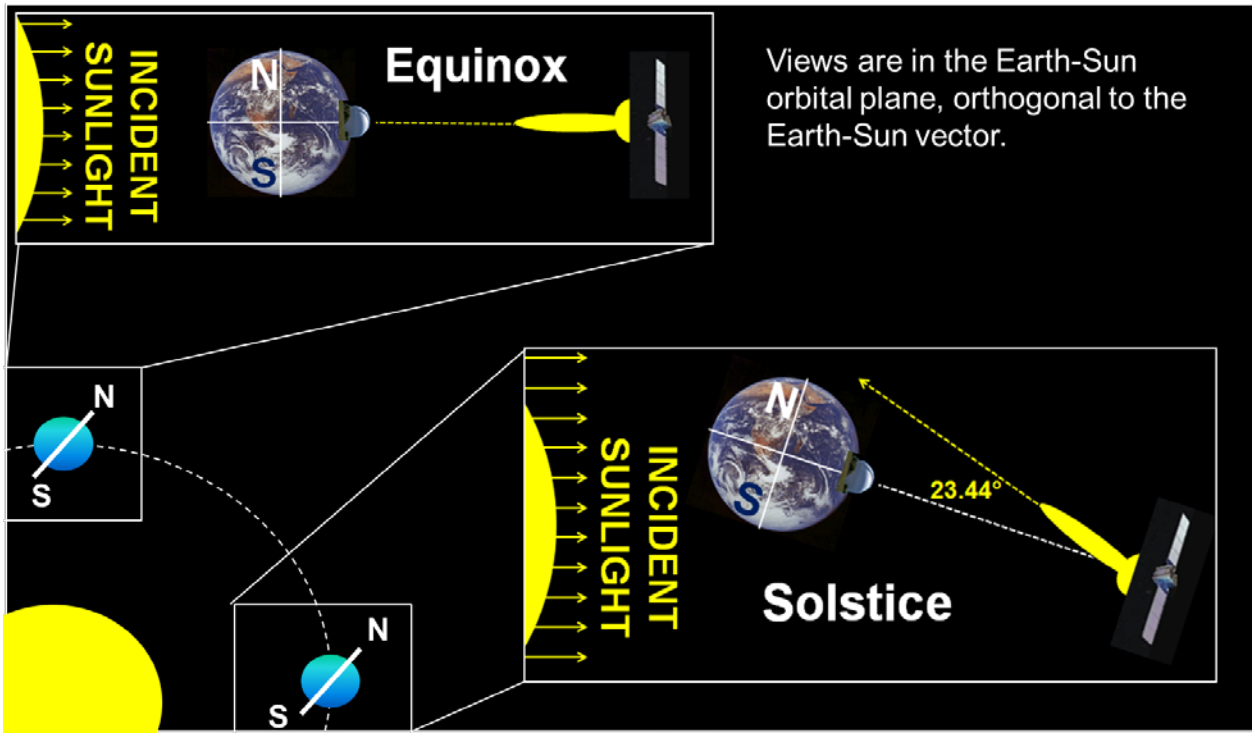

Figure 1: Schematic of the geometrical effect that results in a seasonal effect on the measured reflectance of a 3-axis stabilized GEO satellite, when measured at Equinox, Solstice, and other times of the year. The reflectance function of the satellite is represented by the yellow-colored shapes shown near the satellites. Near Equinox, peak reflectance from solar panels is expected to be observable.

2. THEORETICAL BACKGROUND OF THE SEASONAL EFFECTS MODELS

As previously mentioned, analysis of multi-filter photometric observations of approximately 115 GEO satellites collected over the past 8 years has led to a qualitative understanding of the effects that seasonal illumination changes cause when looking at the reflected sunlight from stable satellites. The most dramatic seasonal effects occur for Solar Phase Angles (PA) near glint. For the concept of Phase Angle, we employ the east/west (e/w) or longitudinal component of the total Solar Phase Angle since there are a number of analytical advantages in the analysis of Geostationary objects. True glints occur when the normal to a main solar panel structure lies along the bisecting angle of the sensor-satellite-sun orientation. For what is typically referred to as a Canonical satellite the bisecting angle is nearly zero and there will be one centralized, PA≈0 ^{o}, peak in the measured light curve.

We are not concerned with direct glints in this paper as they are very complicated and we do not have sufficient data to understand them. However, we *are* interested in modeling near glint conditions, such as those that occur near the bisecting angle of the sensor-satellite-sun, at times of the year other than those when direct glints are conspicuous.
Our model is empirical. We have found that we can effectively correct for seasonal changes by adding varying amounts of magnitude in order to adjust to a standard day of the year. For example, if one wants to test for a change detection in observations made of a given Canonical satellite in January and then of the same satellite one month later, one needs to add brightness (subtract magnitude) to the PA ≈ 0^{o} region for the January observations, knowing that the February observations will be brighter. If we did not make this kind of adjustment, change detection algorithms would lose precision or fail. A note about adding magnitudes rather than fluxes: Since our model is empirical, in our model we violate energy conservation, and we do not have a requirement to conserve flux. More on this point will be discussed when we describe implementation of the model to data sets. Adding varying magnitude corrections is appropriate with respect to the observations in which the magnitude system is used to represent brightness values.

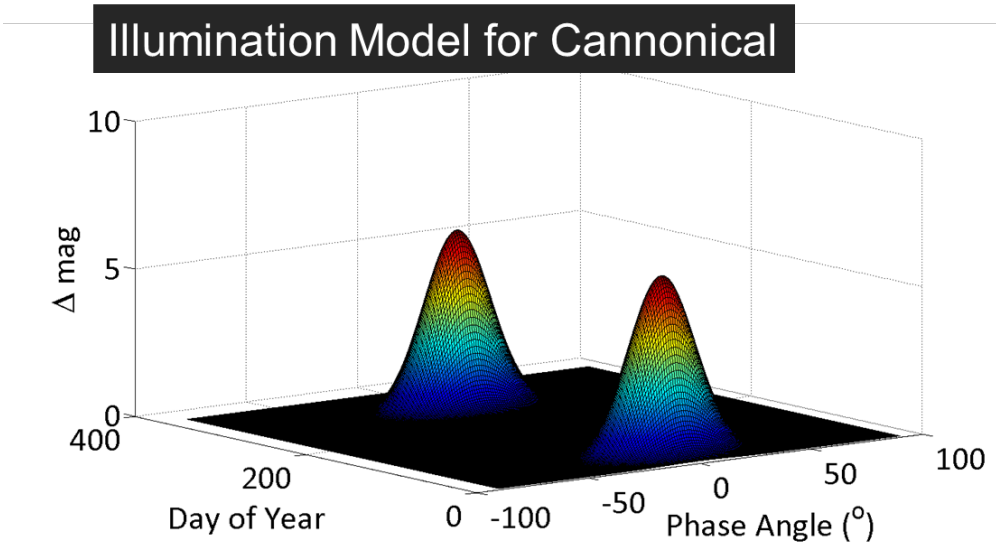

Figure 2: Theoretical model of a Canonical Satellite, where Magnitude is plotted as a function of Solar Phase Angle (PA) and Day of Year (DOY).

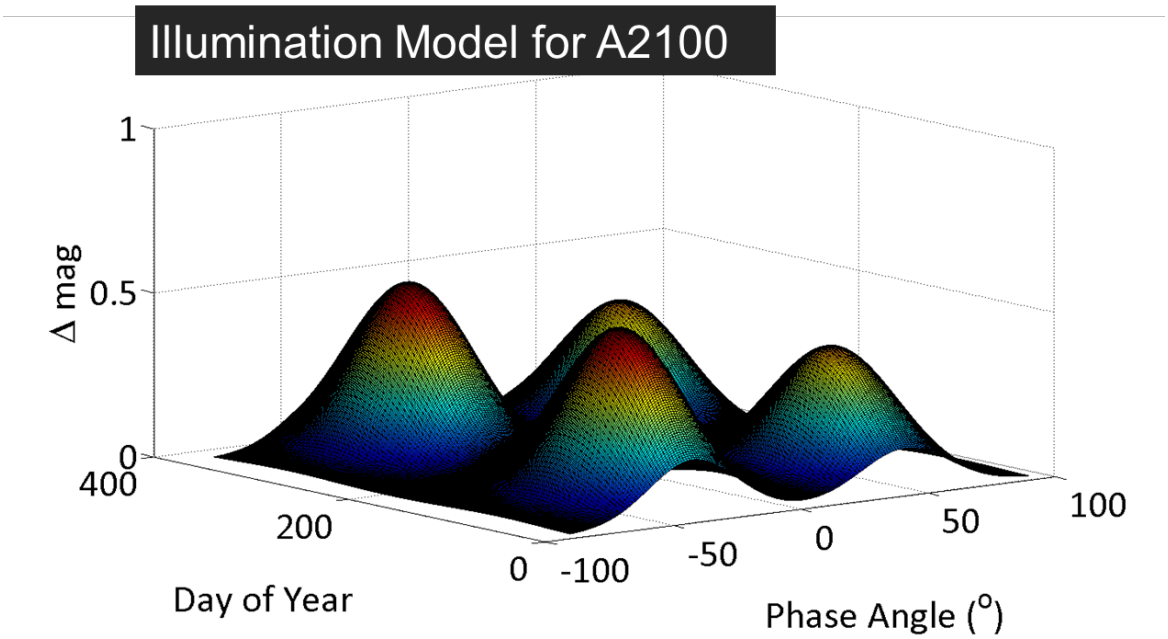

Figure 3: Theoretical model of a Lockheed Martin A2100 Satellite, where Magnitude is plotted as a function of Solar Phase Angle (PA) in degrees and Day of Year (DOY) in units of days.

Our models are based on Gaussian curves and have widths, w_x, of approximately 25^o in the e/w direction and w_y of approximately 19^o, or 40 days, in the n/s direction. Amplitudes, A_1 and A_2, which we allow to be different, typically lie in the 1 to 3 magnitude range. The e/w centers of the Gaussians can be adjusted for solar panel offsets, c_{x1} and c_{x2}, and the n/s centers can be adjusted for slight tilts relative to the satellite major axis, i.e. the axis most nearly aligned to the two main panel structures, relative to the polar axis. With a multiple Gaussian model, we can account for space objects such as the Lockheed Martin A2100 bus type in which the two solar panel structures usually have large offsets – one panel pointing 20^o east of the sun and the other 20^o west of the sun (see Fig. 3).

Optimization of the model is accomplished by calculating a least squares fit to the data and numerical integral of the data minimized with respect to a constant, *E* which represents the conservation of energy constraint. We perform minimization in a manner consistent with the method of Lagrange multipliers, where α is the parameter that represents scale differences between the two optimization constraints. The figure of merit we optimize is given by Eq. 1.

$$J(m_{mod}) = \sum (m_{meas.} - m_{mod.})^2 + \alpha \left(E - \iiint H_0 10^{-m_{mod.}/2.5} d\theta dt d\lambda \right)^2 \quad \text{(Eq. 1)}$$

In Eq.1 m_{mod} is the model magnitude, a quantity we find by optimization. The measured magnitude is represented by $m_{meas.}$, θ is the sensor field of view, t is observation time, and λ is wavelength. Typically H_0 is taken as 2.75e-5ergs/cm^2-s-μm for observational data. Note that the parameter α must account for the unit differences in the term on the left-hand side and the term on the right hand side, in addition to balancing the two optimization constraints for best fit. If α is taken to be zero, only the term on the left-hand side is employed for optimization of J(m_{mod}). In practice minimization of Eq. 1 for α permits approximate energy conservation. When the measurements do not conform to energy conservation constraints, it is necessary to enforce energy conservation. However, this brute force approach to energy conservation modifies the measured values in a way that may negate photometric calibration. We find the energy conservation constraint especially difficult to enforce when glints are conspicuous in the data. Modeled data in the DTV-9s results shown in the next section disobeys energy conservation, but does so only mildly, with less than 1% excursions. The excursions we describe are calculated as the standard deviation in integrated energies divided by the mean of integrated energies, for all available light curves.

As previously described, the model for seasonal correction is a function that we typically represent as a double Gaussian, with peaks at c_{x1} and c_{x2}, and widths w_x and w_y. We have to optimize the model for eight parameters, α, c_{x1}, c_{x2}, A_1, A_2, w_x, w_y, an overall offset in magnitude, and a baseline light curve – typically assumed to be the light curve at or near solstice. Minimization is performed numerically in Matlab using the fminsearch function. [f]minsearch uses the simplex search method of Lagarias et al. [5]. The fminsearch routine finds local minima and is therefore highly dependent on initial conditions. Thus, in implementing fminsearch we test a variety of initial conditions before arriving at the determined minimal set of parameters.

3. APPLICATION OF THE SEASONAL EFFECTS MODEL AND RESULTS

Figure 4 shows an optimized model derived from DTV-9s data.

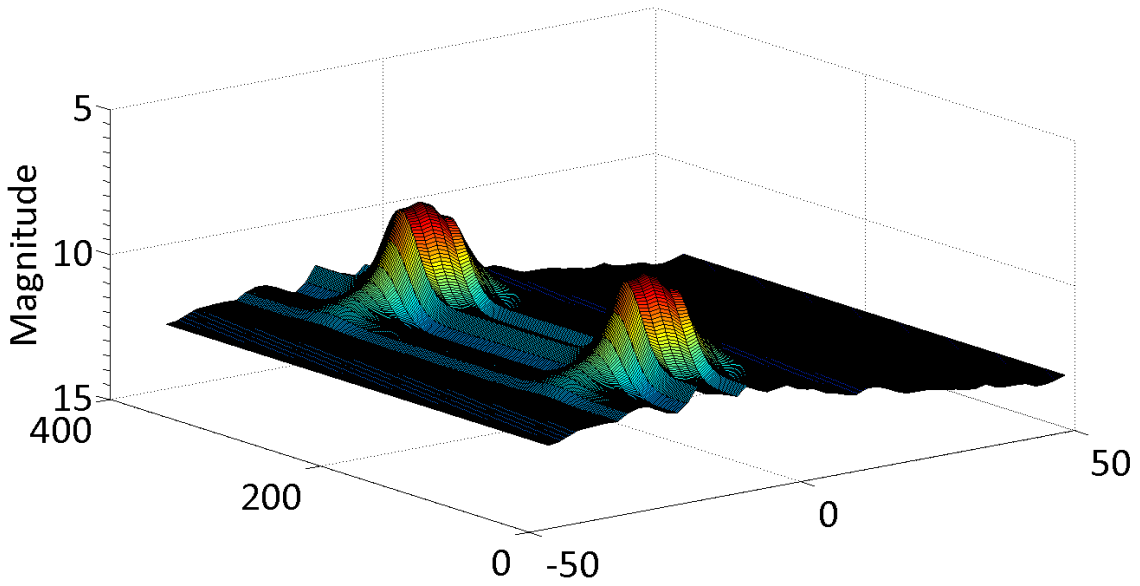

Figure 4: Derived model canonical satellite based on measurements of DTV-9s.

Application of the model permits interpretation of seasonal affects in data, as demonstrated in Figure 5 for measured DTV-9s data. Application of a different, but similarly determined model for a simulated canonical satellite data is shown in Figure 6.

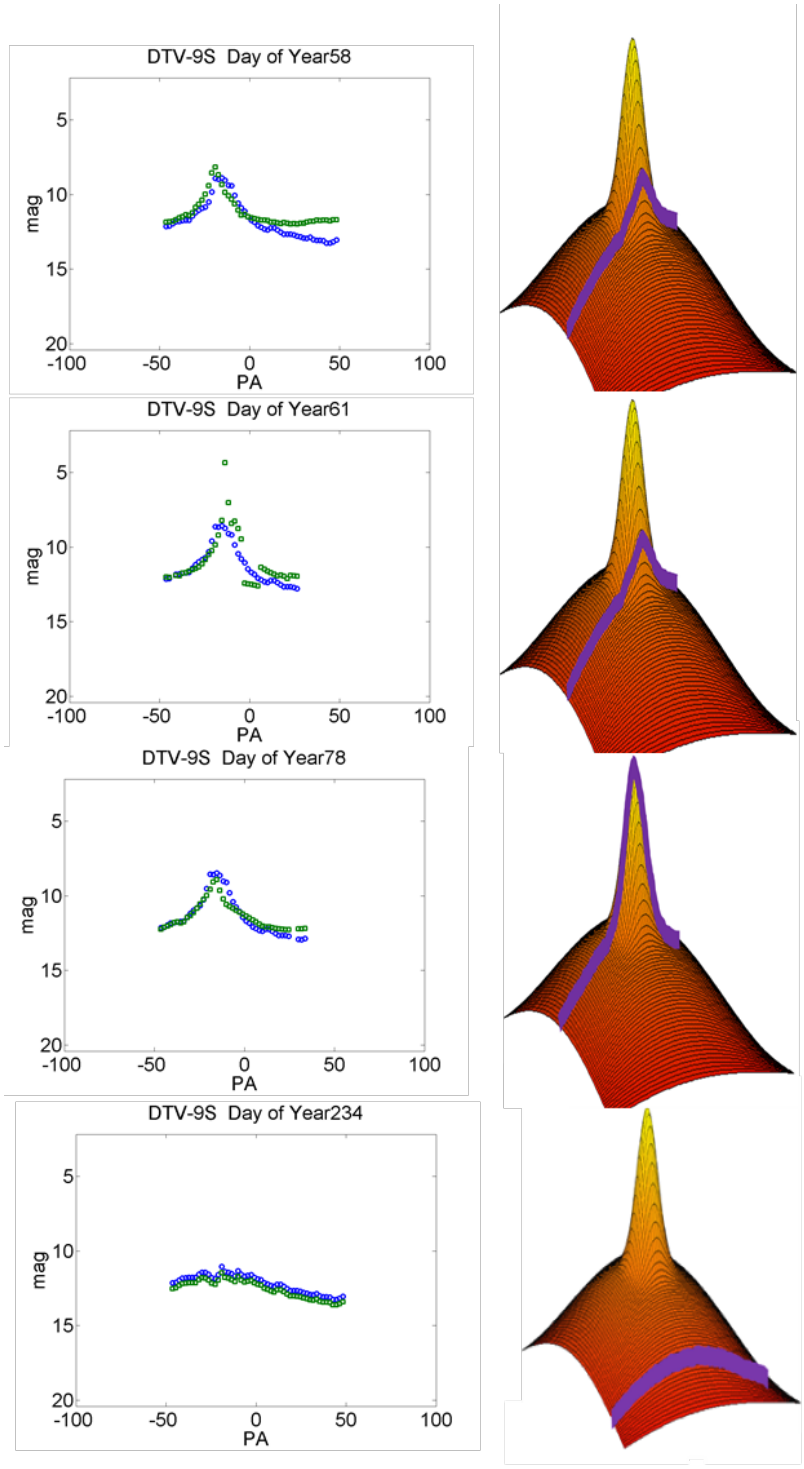

Figure 5: (left) Green circles are measured data points of DTV-9s and blue circles are results of a model, plotted for comparison. (right) Schematic of a theoretical reflectance function with the purple line representing the measured light curve at given time of the year.

In Figure 5, plots on the left hand side show measured DTV-9s data points and model results. On day 61, a large glint from an unknown feature of the satellite is conspicuous, and deviations from the model are observed as the model does not account for this secondary glint. In future investigations a more sophisticated model may be used that could account for the large secondary glint, however with available data we do not yet have enough information

to construct that model. The DTV-9s data shown was collected at Kirtland AFB in New Mexico, and note that, for sensors in the 20^o to 40^o latitude range of the northern hemisphere, the direct glints occur approximately three weeks on the winter side of the equinoxes, i.e. in mid-October and late February/early March.

On day 234 the model and data match near-perfectly, as this is on a date nearing solstice. At solstice, there is little expected contribution from the solar panels, and the model reduces to a baseline light curve with only minor modification. The baseline light curve is the light curve at day 234 and any observed differences between measurement and model in the lower-most plot of Fig. 5 are due to the empirical model.

On the right in Figures 5 and 6 are cartoons of a theoretical reflectance function plotted as a surface with brightness in the z-direction and angles in the two-dimensional plane representing the e/w solar phase angle and the n/s phase angle. The purple line in the schematic represents the measured light curve at the given time of the year; it changes due to the previously mentioned geometry of the satellite relative to the earth and sun during different seasons.

In Figure 6, plots on the left hand side show simulated Canonical data points and model results. On day 355, near solstice, the model and data match near perfectly, as this is the case near solstice, when there is little expected contribution from the solar panels, and the model is a baseline light curve with only minor modification. The baseline light curve is the light curve at solstice.

On the right in Figure 6 are cartoons of a theoretical reflectance function plotted as a surface with brightness in the z-direction and angles in the two-dimensional plane representing the e/w solar phase angle and the n/s phase angle.

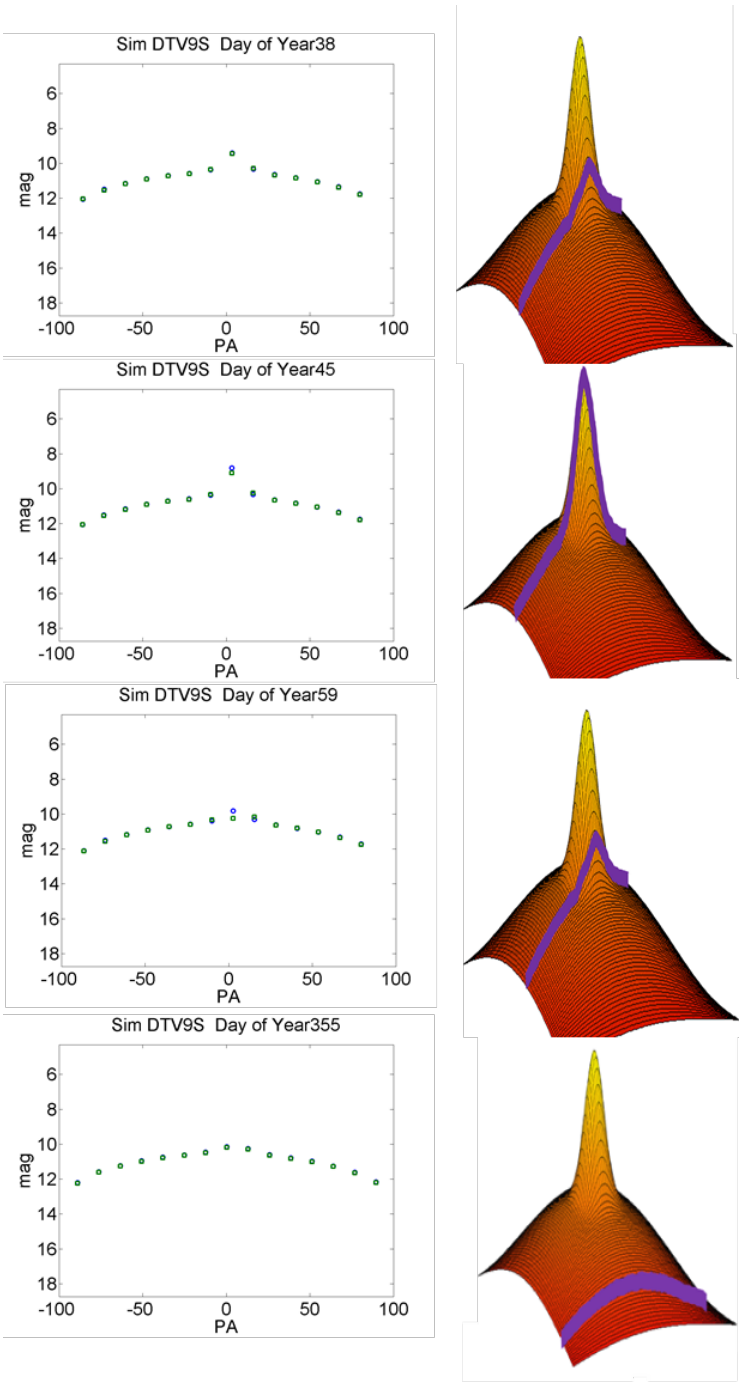

Figure 6: (left) Green circles are simulated data points of a Canonical satellite and blue circles are results of an optimized model plotted for comparison. (right) Schematic of a theoretical reflectance function with purple line representing the measured light curve at given time of the year.

4. DISCUSSION

Results of application of an empirical seasonal model to DTV-9s data demonstrate that such a model can be successfully used to describe large changes between light curves measured for the same 3-axis stabilized satellite during different times of the year. Furthermore, the successful application of the model demonstrates that the seasonal effects represent a cardinal change in the light curve over the course of a year. This result has application

to classification of light curves, which may require seasonal effects modeling for reliable characterization and for change detection in light curves, where changes in the light curve over the course of a year will be evident and interpretable.

The results from application of an empirical seasonal model to simulated Canonical satellite data amplify the results demonstrated with measured data, confirm intuition, and strongly suggest how one must proceed if they wish to use detailed satellite modeling for interpretation of light curves. This last point regarding the interpretation of light curves via satellite modeling implies that the orbits and lighting conditions are key parameters for accurate light curve simulation.

Future work will include more comprehensive models that may incorporate detailed satellite models. Observations of significant secondary glints, such as the one observed in the DTV-9s data strongly suggest that observational data is required for informing the models. Future work will also include collection of more measurements of the type exhibited in this paper.

5. REFERENCES

1 J. Murray-Krezan, S. A. Gregory, W. C. Inbody, A. Dentamaro, and P. Dao, "Automated Characterization of Three-Axis Stabilized GEOs Using Non-Resolved Optical Observations," MIT LL Space Control Conference, 2012.
2 A. B. Chaudhary, T. Payne, S. A. Gregory, and P. Dao, "Fingerprinting of Non-resolved Three-axis Stabilized Space Objects Using a Two-Facet Analytical Model," AMOS Tech Conference 2011.

3 D. Hall, B. Calef, K. Knox, M. Bolden, and P. Kervin, "Separating Attitude and Shape Effects for Non- resolved Objects," AMOS Technical Conference 2007.

4 Stephen A. Gregory, Tamara E. Payne, Maj. Laura Durr, Daniel Senft, Shawn Sawyer, John Klosterman, and Edwin Pease, "Comparisons Between TASAT Simulations and Color Photometry Observations of GEOs", 2008 SSA and Missiles Conference, Maui.

5 Matlab R2011b help files; Lagarias, J.C., J. A. Reeds, M. H. Wright, ad P. E. Wright, "Convergence Properties of the Nelder-Mead Simplex Method in Low Dimensions," *SIAM Journal of Optimization*, Vol. 9 Number 1, pp. 112-147, 1998.